Resource

Cell Host & Microbe

Comprehensive Mapping of HIV-1 Escape from a Broadly Neutralizing Antibody

Graphical Abstract

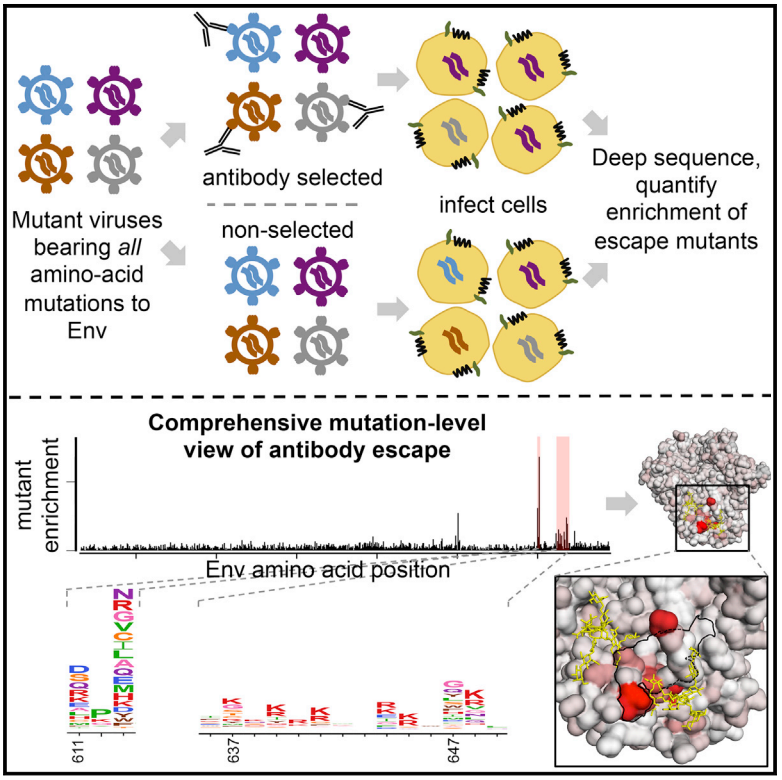

Authors

Adam S. Dingens, Hugh K. Haddox, Julie Overbaugh, Jesse D. Bloom

Correspondence

joverbau@fredhutch.org (J.O.), jbloom@fredhutch.org (J.D.B.)

In Brief

Dingens et al. developed a massively parallel approach to quantify how all mutations to HIV Env affect antibody neutralization in the context of replication-competent virus. They applied this approach to the antibody PGT151, validated the results with neutralization assays, and explored the biochemical basis of HIV escape from this antibody.

Highlights

- HIV antibody-escape mutants were mapped in a single massively parallel experiment
- The high-throughput results correlated with individual neutralization assays
- Escape mutants not found by approaches such as alanine scanning were identified
- The results provide insight into the biochemical basis of antibody escape

Dingens et al., 2017, Cell Host & Microbe *21*, 777–787
June 14, 2017
http://dx.doi.org/10.1016/j.chom.2017.05.003

Cell Host & Microbe
Resource

Comprehensive Mapping of HIV-1 Escape from a Broadly Neutralizing Antibody

Adam S. Dingens,[1,2,3] Hugh K. Haddox,[1,3] Julie Overbaugh,[2,*] and Jesse D. Bloom[1,4,*]
[1]Division of Basic Sciences and Computational Biology Program
[2]Division of Human Biology and Epidemiology Program
Fred Hutchinson Cancer Research Center, Seattle, WA 98109, USA
[3]Molecular and Cellular Biology PhD Program, University of Washington, Seattle, WA 98195, USA
[4]Lead Contact
*Correspondence: joverbau@fredhutch.org (J.O.), jbloom@fredhutch.org (J.D.B.)
http://dx.doi.org/10.1016/j.chom.2017.05.003

SUMMARY

Precisely defining how viral mutations affect HIV's sensitivity to antibodies is vital to develop and evaluate vaccines and antibody immunotherapeutics. Despite great effort, a full map of escape mutants has not been delineated for an anti-HIV antibody. We describe a massively parallel experimental approach to quantify how all single amino acid mutations to HIV Envelope (Env) affect neutralizing antibody sensitivity in the context of replication-competent virus. We apply this approach to PGT151, a broadly neutralizing antibody recognizing a combination of Env residues and glycans. We confirm sites previously defined by structural and functional studies and reveal additional sites of escape, such as positively charged mutations in the antibody-Env interface. Evaluating the effect of each amino acid at each site lends insight into biochemical mechanisms of escape throughout the epitope, highlighting roles for charge-charge repulsions. Thus, comprehensively mapping HIV antibody escape gives a quantitative, mutation-level view of Env evasion of neutralization.

INTRODUCTION

HIV's rapid evolution enables it to outpace even the exceptional adaptive capacity of the humoral immune system. Although the immune system is usually outmatched in this evolutionary arms race, leading to viral persistence, infected individuals occasionally develop antibodies capable of neutralizing diverse viral strains. While these broadly neutralizing antibodies (bnAbs) do not control infection in the individual in whom they arise, their identification has motivated efforts in rational vaccine design and antibody immunotherapeutics. For example, epitope mapping of bnAbs has revealed conserved sites of vulnerability on HIV's envelope glycoprotein (Env), and a leading vaccine strategy is to design immunogens that elicit an antibody response targeting these conserved sites (Wu and Kong, 2016). bnAbs are also being tested in both prophylactic and therapeutic settings. Numerous studies in animal models have shown proof of concept that passively infused bnAbs can protect against infection (Hessell et al., 2009; Mascola et al., 1999, 2000; Moldt et al., 2012; Parren et al., 2001; Pegu et al., 2014; reviewed in Pegu et al., 2017) and therapeutically suppress viremia during infection (Barouch et al., 2013; Horwitz et al., 2013; Klein et al., 2012; Shingai et al., 2013; reviewed in Margolis et al., 2017). Similar bnAb-based immunotherapies are being tested in humans, with some early studies showing a transient reduction in viral load or delay of viral rebound after treatment interruption in some individuals (Bar et al., 2016; Caskey et al., 2015, 2017; Lynch et al., 2015a; Scheid et al., 2016).

Despite the impressive breadth and potency of bnAbs in vitro, HIV can eventually evade them in vivo. Viral isolates from individuals who develop bnAbs are typically resistant to neutralization, and resistance arises when bnAbs are administered to infected animal models (Klein et al., 2012; Poignard et al., 1999; Shingai et al., 2013) or humans (Bar et al., 2016; Caskey et al., 2015, 2017; Lynch et al., 2015a; Scheid et al., 2016; Trkola et al., 2005). It is therefore important to prospectively identify all *env* mutations that affect the sensitivity to a bnAb. However, this can be challenging, in part because bnAbs often target complex conformational and glycosylated epitopes. To date, a complete set of HIV escape mutations has yet to be elucidated for any antibody.

The limited observational studies of viral escape from bnAbs to date likely reveal only a fraction of the full repertoire of escape mutations. Structural studies provide atomic-level views of the antibody-antigen footprint, but fail to reveal which interactions are necessary for neutralization and which mutations disrupt these interactions. Indeed, it has long been appreciated that binding energetics are often concentrated at select sites in the protein-protein interface (Clackson and Wells, 1995; Cunningham and Wells, 1993), and mutations at Env residues that participate in crystal-structure-defined interactions do not always affect bnAb binding and neutralizing (Falkowska et al., 2012; Li et al., 2011). Because structures do not functionally define escape mutations, researchers often generate and interrogate single amino acid mutants in binding or neutralization assays. This approach is so labor intensive that it has only been applied to a fraction of the sites in Env, and typically to only one or a few mutations—often to alanine—at these sites.

We have applied a deep mutational scanning-based approach to comprehensively map all mutations to Env that enable HIV to escape from a bnAb. This approach, mutational antigenic profiling, involves creating libraries of all single amino acid

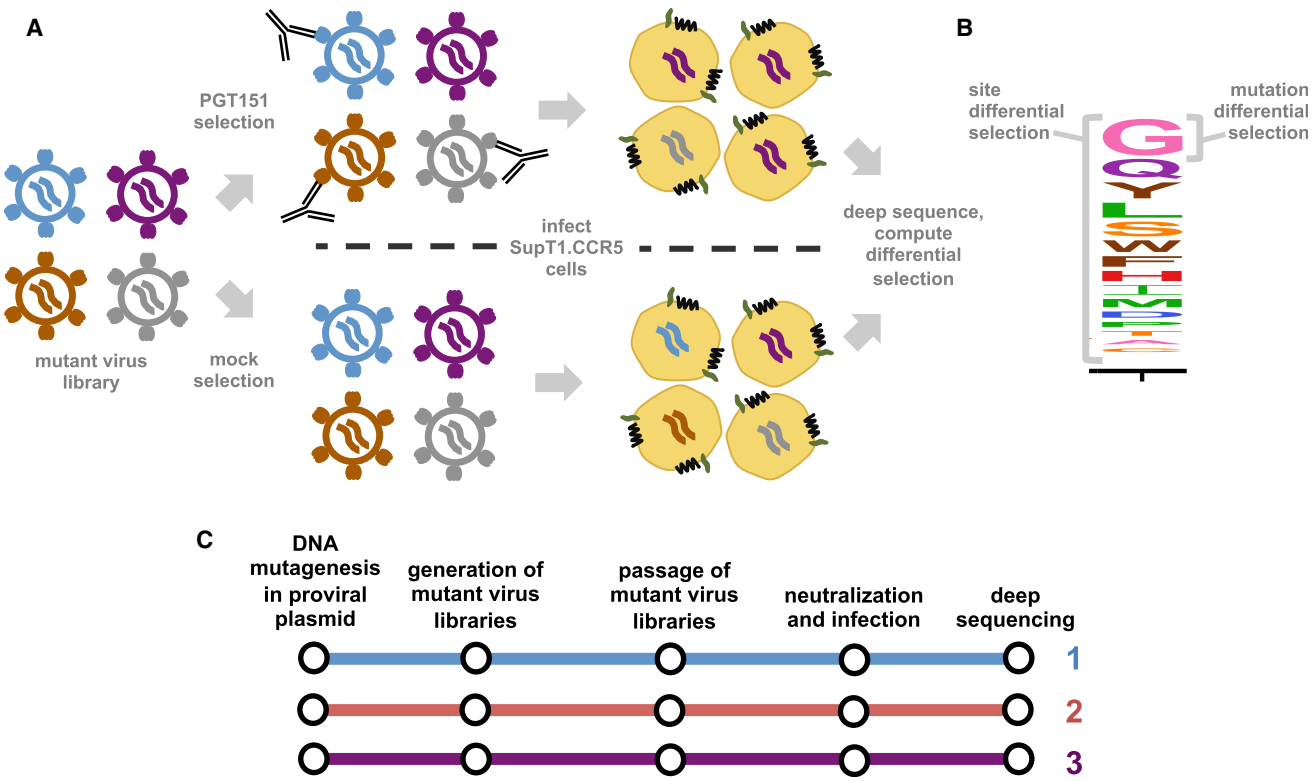

Figure 1. Schematic of Mutational Antigenic Profiling

(A) Mutant virus libraries of HIV, which have been passaged in SupT1.CCR5 cells and thus should encode all single amino acid mutants to Env compatible with viral replication, are incubated with and without an anti-HIV antibody, and then infected into SupT1.CCR5 cells. After viral entry and reverse transcription, cDNA is isolated and *env* is deep sequenced. The differential selection exerted by the antibody is quantified as the logarithm of the frequency of each mutation relative to wild-type in the antibody-selected condition compared to the control condition.

(B) A logoplot visualizing the differential selection at a single site. The height of each letter is proportional to the differential selection for that amino acid mutation. The site differential selection is the sum of all mutation differential selection values at that site.

(C) The entire mutational antigenic profiling process was completed in biological triplicate, starting from generation of three independent *env* mutant libraries in the context of proviral plasmids.

mutants of Env in the context of replication-competent HIV (Haddox et al., 2016), selecting for mutations that promote antibody escape, and using deep sequencing to quantify the enrichment of each mutation. It is conceptually similar to a strategy recently used by Doud et al. (2017) to completely map the escape of influenza A from anti-hemagglutinin antibodies. Our work comprehensively profiles HIV escape from bnAb neutralization in the context of actual virus, distinguishing it from previous deep mutational scanning experiments that have used yeast or cell-surface display to identify Env variants that bind germline-encoded bnAb progenitors (Jardine et al., 2016; Steichen et al., 2016). The map of escape mutations that we generate provides a complete view of the functional interface between Env and a bnAb, and suggests biochemical mechanisms of escape that are not readily apparent from the incomplete data provided by traditional mapping approaches.

RESULTS

Overview of Mutational Antigenic Profiling

To define all single amino acid mutations to Env that increase resistance to antibody neutralization, we implemented the mutational antigenic profiling approach in Figure 1. This approach relies on creating libraries of full-length proviral clones encoding all possible mutations in *env* and passaging these libraries in T cells (Haddox et al., 2016). The result is a library of replication-competent HIV encoding all functionally tolerated mutations in Env. This mutant library is then incubated with and without antibody and used to infect target cells. After entry, the frequency of each mutation in the infected cells is quantified by deep sequencing (Figure 1A). The "differential selection" that the antibody exerts on a mutation is defined as the logarithm of that mutation's enrichment in the antibody-selected condition relative to the control, and selection for enriched mutations is plotted in logoplots as shown in Figure 1B. The entire experiment was performed in biological triplicate beginning from independent generation of the proviral plasmid mutant libraries (Figure 1C).

Generation and Deep Sequencing of Mutant Virus Libraries

We applied mutational antigenic profiling to a virus relevant to HIV transmission by generating the mutant libraries in the context of an *env* (BF520.W14M.C2) from a subtype A virus isolated shortly after mother-to-child transmission in an infant who went on to

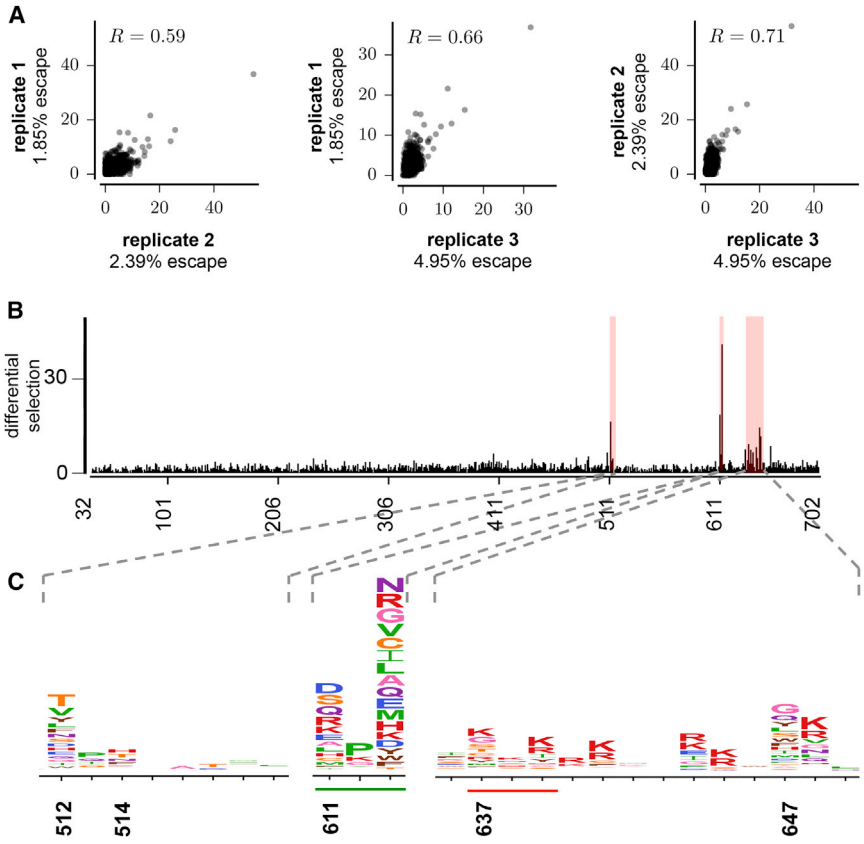

Figure 2. Reproducibility of Mutational Antigenic Profiling

(A) Correlation of site differential selection across biological replicates. Each point indicates the selection at one of the 661 Env sites; plots also show the Pearson correlation. Percent escape was calculated by using droplet-digital PCR to measure the number of viral genomes in the antibody-selected versus control sample.

(B) The site differential selection, averaged across replicates, is plotted across the Env sequence. See Figure S3 for data from individual replicates.

(C) Logoplots showing mutation differential selection in strongly selected regions. Mutations at numbered sites have previously been shown to reduce PGT151 neutralization sensitivity in other viral strains. From left to right: the fusion peptide, the 611 glycosylation motif (underlined in green), and the 637 glycosylation motif (underlined in red) and HR2 domain. Mutations can eliminate an N-linked glycan if they disrupt the N-X-S/T glycosylation motif, where X can be any amino acid except proline.

rapidly develop a bnAb response (Goo et al., 2012; Simonich et al., 2016; Wu et al., 2006). We introduced all possible codon-level mutations to gp120 and the extracellular portion of gp41 (Env residues 32–703) in the context of a proviral plasmid. We did not mutagenize Env's signal peptide or cytoplasmic tail, as these are not direct targets of neutralizing antibodies but play a role in regulating Env cell-surface expression (Chakrabarti et al., 1989; Li et al., 1994; Yuste et al., 2004). Sanger sequencing of individual proviral clones revealed that the number of codon mutations per clone followed a Poisson distribution with a mean of 1.1 mutations/clone, and the mutations were relatively uniformly distributed along the length of Env (Figures S1 and S2).

We used deep sequencing to measure the frequency of each mutation in the mutant proviral plasmid, as well as in the mutant virus libraries with and without antibody selection. Because any given mutation is rare, we performed deep sequencing using a barcoded-subamplicon approach that tags individual molecules with unique molecular identifiers during the library preparation to increase accuracy (Doud and Bloom, 2016; Jabara et al., 2011; Wu et al., 2016). Deep sequencing of the mutant proviral plasmids showed that 95% of the 12,559 possible single amino acid mutations (661 mutagenized residues × 19 mutant amino acids) were present in each of the triplicate BF520 plasmid mutant libraries, with 99% present in the three libraries combined. Figure S2 shows that the sequencing error rate is 1.5×10^{-4} mutations/codon (equivalent to 5×10^{-5} mutations/nucleotide) as assessed by sequencing unmutated wild-type proviral plasmid. This error rate is over 10-fold lower than the frequency of codon mutations in the plasmid mutant libraries.

We also quantified the rates of errors associated with viral replication by sequencing wild-type viruses passaged in parallel to each mutant virus library (described below). The rate of errors in these passaged wild-type viruses remained well below the rate of mutations in the virus mutant libraries, allowing us to reliably assess mutation frequencies (Figure S2). In the analyses below, we statistically correct for these errors associated with viral replication as described in the Computation of differential selection section in the STAR Methods.

Comprehensive Profiling of Escape from Antibody PGT151

We chose to profile escape from the bnAb PGT151, which targets a quaternary, cleavage-dependent epitope made up of glycans and protein residues in the gp120/gp41 interface and fusion peptide. This bnAb has been extensively studied, using both structural (Blattner et al., 2014; Lee et al., 2016) and functional approaches (Falkowska et al., 2014; van Gils et al., 2016; Kong et al., 2016; Wibmer et al., 2017).

To generate mutant virus libraries, we transfected the BF520 mutant proviral plasmids into 293T cells and passaged the transfection supernatant in SupT1.CCR5 cells at a low MOI to establish a genotype-phenotype link and purge non-functional mutants. The resulting passaged mutant virus libraries, which we expect to carry virtually all Env amino acid mutations compatible with viral replication, were used to infect cells in the presence and absence of PGT151. We then isolated and deep sequenced viral cDNA from infected cells to determine the frequency of each mutation, and computed the differential selection across Env.

Among the three biological replicates, the site differential selection was well correlated (R = 0.59–0.71; Figures 2A and S3), indicating that the high-throughput experiments yielded

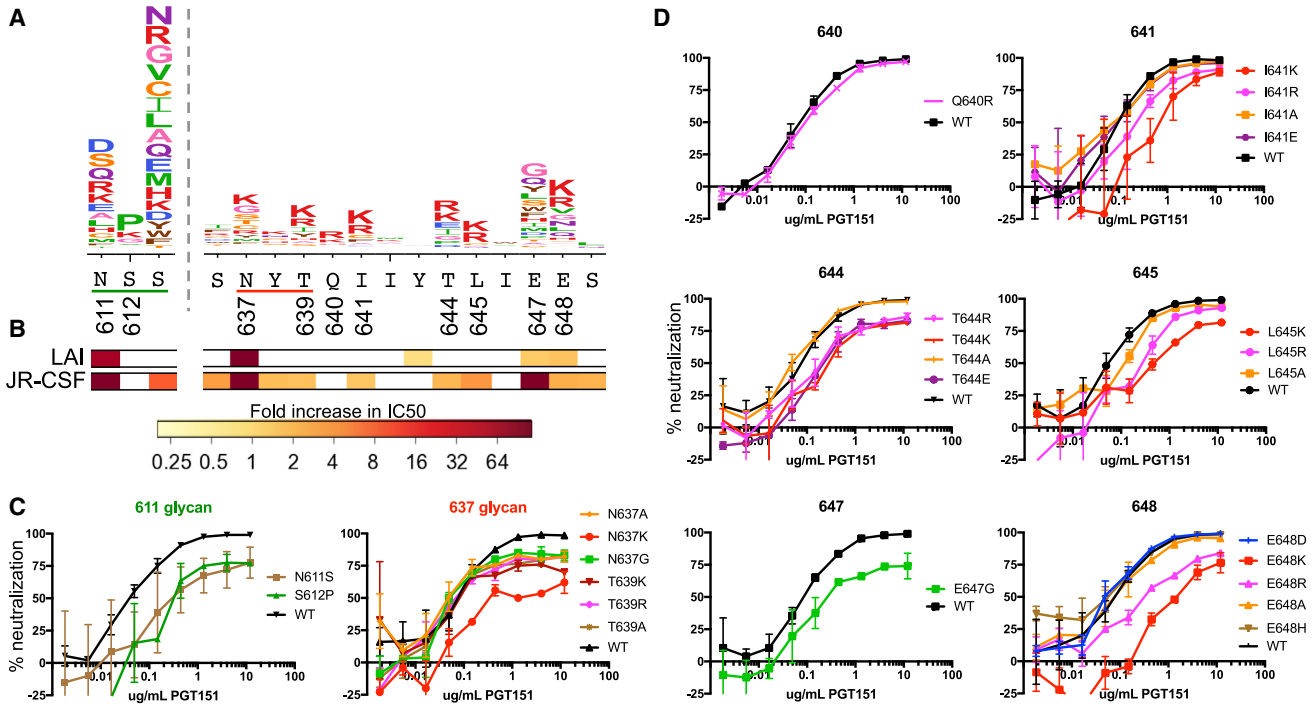

Figure 3. Analysis of the Effect of Individual Amino Acid Changes Identified by Mutational Antigenic Profiling on PGT151 Neutralization

(A) Logoplots showing differential selection. Sites where individual mutations were tested in neutralization assays are numbered, and the 611 and 637 glycosylation motifs are underlined in green and red.

(B) Color bars below the logoplots indicate the results of neutralization assays performed on point mutants (primarily to alanine) of JR-CSF and LAI by Falkowska et al. (2014). The bar at each site is colored according to the fold change in IC_{50} relative to wild-type that a mutation imparted. If multiple amino acids were tested at a site, the site is colored according to the largest effect.

(C) Results of TZM-bl pseudovirus neutralization assays on BF520 Env point mutants that alter the N-linked glycosylation motifs at sites 611 and 637.

(D) Results of neutralization assays at individual residues outside of glycosylation motifs.

In (C) and (D), each plot shows a representative neutralization curve; see Figure S4 for regression curves from replicate assays. Error bars plot the SD of duplicate wells within a single replicate.

reproducible results even when starting with fully independent mutant proviral plasmid libraries.

There was strong selection at sites in the known PGT151 epitope. Figure 2B plots the site differential selection across Env, and Figure 2C displays the escape profiles in regions of strong differential selection. These sites include residues originally mapped by mutagenesis and pseudovirus-neutralization assays: the dominantly targeted 611 glycan, the 637 glycan, and residue 647 (Figures 2B and 2C) (Falkowska et al., 2014). There was also strong differential selection at fusion-peptide sites 512 and 514, which have been mapped as part of the PGT151 epitope by structural (Lee et al., 2016) and functional (van Gils et al., 2016; Kong et al., 2016; Wibmer et al., 2017) methods (Figure 2C). Therefore, our mutational antigenic profiling identified strong selection at epitope sites that have been identified by other approaches.

Validation of Mutational Antigenic Profiling at Previously Mapped Sites

We next used TZM-bl neutralization assays of BF520 pseudoviruses with select mutations that were and were not differentially selected in our mutational antigenic profiling to further examine how well our comprehensive escape profiles predicted neutralization escape (Figures 3 and S4). We first focused on sites that had been previously defined as conferring escape from PGT151, including mutations that disrupt the gp41 glycans at sites 611 and 637. Mutational antigenic profiling revealed strong selection for most mutations that disrupt the 611 glycosylation motif (N-X-S/T, where X can be any amino acid except proline) (Figure 3A). Both the 611 and 637 glycans make extensive contacts with the PGT151 Fab (Lee et al., 2016), and elimination of either can increase the IC_{50} in a number of strains (Falkowska et al., 2014). Of note, there was selection for proline at the central position of the 611 glycosylation motif, but not at the central position in the 637 glycosylation motif (Figure 3A). The 638P mutation was depleted in the mutant virus libraries passaged in the absence of PGT151 selection, and we were unable to generate pseudoviruses bearing this mutation, suggesting that proline is not tolerated (data not shown).

At site 637, some of the glycan knockout mutations are under stronger differential selection than others (Figure 3A). Consistent with the mutational antigenic profiling, the effect of these mutations on neutralization sensitivity in TZM-bl assays varied. According to the mutational antigenic profiling, the most strongly selected mutation at site 637 was to K (Figure 3A). In the neutralization assays, this mutation increased the IC_{50} by 3.7-fold.

A

	Mutational antigenic profiling relative fold enrichment	TZM-bl neutralization	
		Fold increase in IC_{50} relative to WT	Maximum % neutralization
N611S	5.4	5.0	98
S612P	8.0	7.1	81
N637A	1.0	1.1	81
N637K	3.7	4.3	59
N637G	2.8	1.0	80
T639K	4.8	1.5	74
T639R	2.8	1.0	79
T639A	1.4	1.2	78
Q640R	2.6	1.1	98
I641K	5.7	5.8	91
I641R	3.2	2.6	92
I641A	1.4	1.3	101
I641E	1.2	1.4	98
T644R	4.0	2.8	87
T644K	3.2	5.3	80
T644A	1.0	1.1	96
T644E	2.2	2.3	84
L645K	3.8	7.6	90
L645R	3.7	3.3	93
L645A	0.7	1.8	96
E647G	5.3	2.6	74
E648D	0.7	0.9	98
E648K	7.7	7.8	74
E648R	3.7	10.9	104
E648A	1.2	1.5	101
E648H	1.5	1.0	113

<2	>90
2-4	80-90
4-6	<80
6-8	
>8	

B

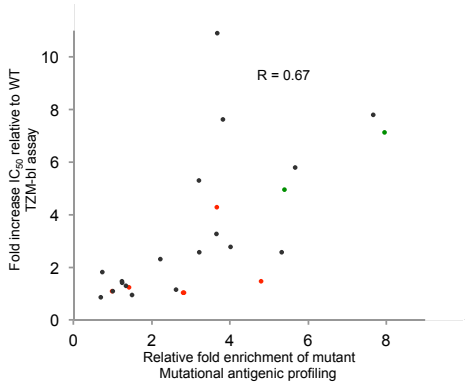

Figure 4. Comparison of Effects of Mutations in Mutational Antigenic Profiling versus TZM-bl Neutralization Assays

(A) Comparisons between fold enrichment in mutational antigenic profiling of each validated mutation (Figure 3), and the fold increase in IC_{50} value relative to wild-type and maximum percent neutralization estimated from replicate neutralization assays.

(B) For each individually tested mutations, the Pearson correlation between the fold enrichment in mutational antigenic profiling and the neutralization assay fold increase in IC_{50} relative to wild-type. Mutations that disrupt the 611 and 637 glycan are shown in green and red, respectively.

Disrupting targeted glycans can also alter neutralization sensitivity by decreasing the maximum percent neutralization; the 637K variant also decreased the maximum percent neutralization to 59% (Figures 3C and 4A). All other tested mutations decreased the maximum percent neutralization of PGT151 to 74%–81% (Figures 3C and 4A) but did not alter the IC_{50}. These results agree with and expand on previous observations; mutations that disrupt the 637 glycosylation motif have been shown to decrease the maximum percent neutralization in JR-CSF, LAI, and JR-FL (Falkowska et al., 2014), and PGT151 often incompletely neutralizes pseudoviruses bearing many different Env variants (McCoy et al., 2015).

Prior work has also shown that mutations at site 647 reduce neutralization sensitivity in some strains (Figure 3B) (Falkowska et al., 2014). Mutational antigenic profiling agreed with these results, revealing strong differential selection for many mutations at site 647. We confirmed the most strongly selected mutation (E647G) mediated escape in a neutralization assay, with IC_{50} fold change of 5.3 (Figure 3D).

Overall, these results show that mutations at previously identified sites that are also mapped by our high-throughput approach indeed have clear effects on neutralization sensitivity in the BF520 variant when tested individually.

The Comprehensive Nature of Mutational Antigenic Profiling Allowed Identification of Additional Sites of Escape

Our mutational antigenic profiling data showed strong selection at several sites where escape mutations have not previously been mapped. As noted above, both our work and prior studies identified escape mutations at site 647, where many different amino acid mutations mediated escape (Figure 3A). In contrast, mutational antigenic profiling also showed selection for mutations to positively charged amino acids at the neighboring site 648, where previous studies did not find effects of mutations to alanine or glycine (Figure 3A; Falkowska et al., 2014). Viruses engineered with E648K and E648R showed substantially reduced sensitivity to PGT151 (IC_{50} fold change of 7.7 and 3.7, respectively), but mutations to a variety of other amino acids (D, A, and H) have no effect (less than 1.5-fold change in IC_{50}) (Figure 3D).

At a number of additional positions in the heptad repeat 2 domain (HR2), including sites 641, 644, and 645, we also observed strong differential selection for predominantly positively charged mutations. Consistent with prior work in other strains (Falkowska et al., 2014), both mutational antigenic profiling (Figure 3A) and pseudovirus neutralization assays (Figure 3D) showed no effect of alanine mutations at these sites. However, the positively charged escape mutations revealed by mutational antigenic profiling indeed reduced neutralization sensitivity when assayed in individual neutralization assays, with fold changes in IC_{50} ranging from 3.2- to 5.7-fold.

Correlation between Mutational Antigenic Profiling and Traditional Neutralization Assays

At each validated site, the ranked order of effects of each mutation on neutralization sensitivity was well correlated between our high-throughput experiments and individual TZM-bl assays (Figures 3 and 4). Across all validated sites, we next asked if our differential selection measures were representative of the true neutralization phenotype. For the BF520 mutations that we tested, the enrichment measured by mutational antigenic profiling is well correlated with the fold change in IC_{50} relative to wild-type from TZM-bl assays (R = 0.67; Figure 4).

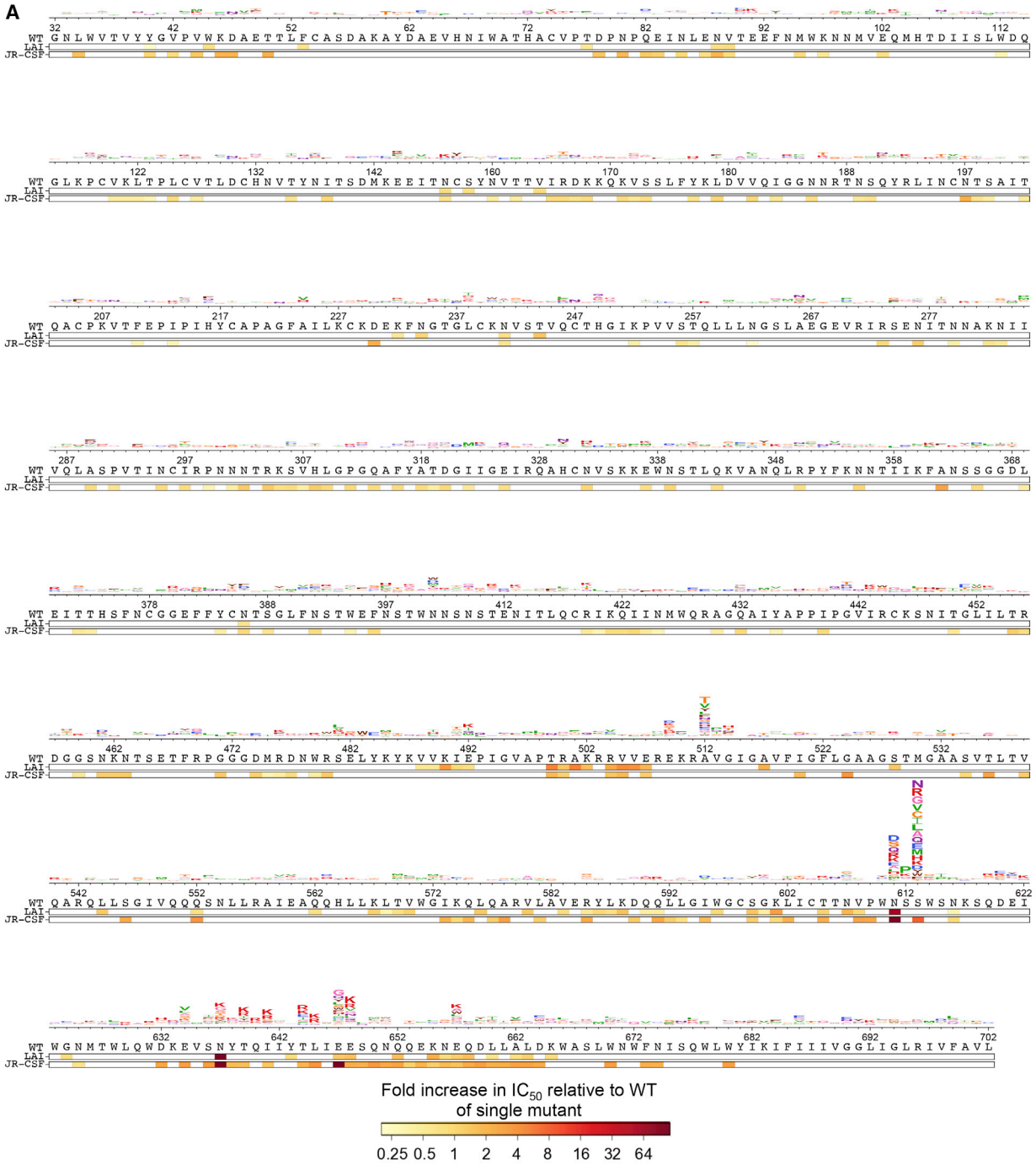

(legend on next page)

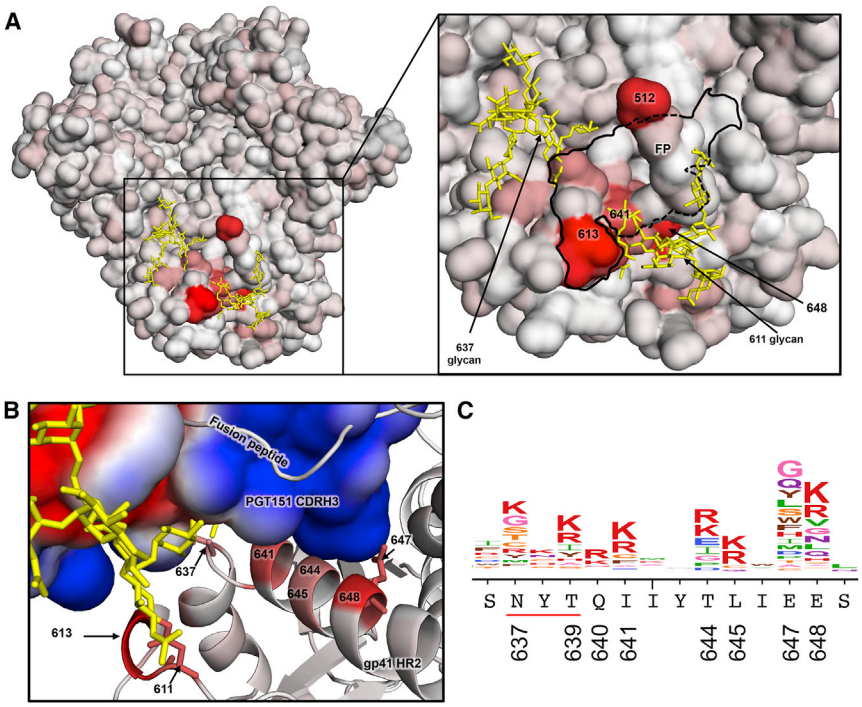

Figure 6. Mutational Antigenic Profiling Combined with Structural Analysis Suggests Escape via the Introduction of Charge Repulsions

(A) The JR-FL EnvΔCT trimer cryo-EM model (Lee et al., 2016) with its surface colored according to the maximum mutation differential selection at each site. The 611 and 637 glycans are shown in yellow. The inset outlines the PGT151 footprint in black, defined as residues that come within 4 Å of the bound PGT151 Fab, with the 611 glycosylation motif residues included for clarity. The bound PGT151 Fab is not shown, and the fusion peptide (FP), which is sequestered into a hydrophobic pocket of bound PGT151, protrudes from the epitope in this view.

(B) A side view of the PGT151 CDRH3-Env interface. Here, the ribbon representation of Env is colored according to the maximum mutation differential selection at each site, while the surface of the bound PGT151 Fab is colored according to the Poisson-Boltzmann electrostatic surface potential (red to blue; negative to positive). The negatively charged side chain of site E647 is shown in stick representation. See Figure S5 for an alternate view of this interface.

(C) Logoplot showing the differential selection of the HR2 domain shown in (B) for reference.

Remarkably, this is within the range of correlations observed between neutralization assays performed on the same sets of viruses by different laboratories (Todd et al., 2012). Further, the IC_{50} only partially summarizes the information in a neutralization curve, as mutations also altered the maximum percent neutralization (Figure 4A). Many of the mutations that exhibit the poorest correlation between fold change in IC_{50} and enrichment in mutational antigenic profiling strongly affect the maximum percent neutralization (Figure 4A), suggesting that the differential selection measures captured both neutralization-curve phenotypes. Of note, the mutations that result in incomplete neutralization include those that eliminate targeted glycans as well as those that are in the Env-PGT151 protein interface. These data agree with observations that PGT151 often incompletely neutralizes *env* isolates, with PGT151 reaching less than 80% maximum percent neutralization for 26% of viral isolates tested (Falkowska et al., 2014; McCoy et al., 2015).

Comparison of our Escape Profiles to the Original Gene-wide Functional Mapping of PGT151

The original residue-level mapping of the PGT151 epitope was based on neutralization of two large panels of pseudovirus mutants (Falkowska et al., 2014). This work provided a large dataset against which we can benchmark our results and contrast our high-throughput measurements with results from traditional approaches. Figure 5A shows the differential selection that PGT151 exerts on every mutation at every site in Env with data from the original mapping of PGT151 shown in color bars below. In a single massively parallel experiment, we have recapitulated these original results (identifying sites 611, 637, and 647), identified sites mapped in subsequent studies (sites 512 and 514), and revealed additional sites of escape in the HR2 domain. In contrast, examining mutations one by one in neutralization assays is exceedingly low throughput—for instance, even with herculean effort (Falkowska et al., 2014), traditional approaches have only managed to test mutations at a fraction of the sites in Env (Figure 5B). The discrepancy in completeness is even more apparent when considering the fact that testing one amino acid mutation at a site does not reveal the effects of other mutations at the same site. Whereas our study examined all 12,559 amino acid mutations, prior work has managed to examine only a small fraction of these mutations (Figure 5B).

Structural Insights into Biochemical Basis of Escape from PGT151

We can interpret the differential selection measured by mutational antigenic profiling in the context of known structural information about the interface between Env and PGT151. Figure 6A maps the maximum mutation differential selection at each site onto the cryo-EM model of JR-FL Env trimer bound by

Figure 5. Complete Mapping of Escape from PGT151

(A) Differential selection for the entire mutagenized portion of Env. For systematic comparison, we plotted data from the original single residue-level mapping utilizing large panels of predominantly alanine scanning mutants of LAI and JR-CSF (Falkowska et al., 2014); sites where mutations were tested are colored according to the fold increase in IC_{50} relative to wild-type as in Figure 3. The wild-type amino acid is also shown for each site.

(B) The number of sites and mutations tested for ability to replicate and escape PGT151 neutralization in the BF520 strain using mutational antigenic profiling compared with the number of sites and mutations tested using traditional approaches (mutagenesis and TZM-bl neutralization assays) applied to the JR-CSF and LAI strains in the original functional mapping of PGT151 (Falkowska et al., 2014).

PGT151 Fabs (Lee et al., 2016). The strongest differential selection maps to the structurally defined PGT151 epitope. The positively charged third complementary determining region of the heavy chain (CDRH3) of PGT151 extends into the negatively charged inter-protomer cavity at the interface between gp120 and the HR2 domain of gp41 (Figure S5). There is differential selection predominantly for mutations to positively charged amino acids on the CDRH3-proximal side of the HR2 alpha helix (Figures 6 and S5), suggesting that escape in this portion of the epitope is mediated by the introduction of charge-charge repulsions.

The importance of charge-charge repulsions may extend to the glycosylated residue 637 (Figure S5C). While any mutation that eliminates the 637 glycan results in incomplete neutralization, the introduction of a positively charged lysine results in a large reduction in both maximum percent neutralization and an increase in IC_{50} (Figures 3C and 5A). Similarly, mutating site 637 to lysine has a larger effect than mutating it to alanine in multiple other strains (Falkowska et al., 2014).

Indeed, it may be possible to conceptually distinguish between sites where almost any mutation mediates escape by *eliminating* key antibody-Env interactions, versus sites where only a few mutations mediate escape by *introducing* steric or electrostatic clashes. For instance, site 647 appears to fall into the first category, with both our mutational antigenic profiling of BF520 (Figure 6C) and prior work with JR-CSF (Falkowska et al., 2014) suggesting that many mutations mediate escape. Indeed, the cryo-EM model suggests that the E at site 647 may interact with positively charged portions of PGT151's HCRD3 arm (Figures 6B and S5C). In contrast, at many of the sites of escape revealed by mutational antigenic profiling, selection is for mutations to positively charged amino acids that are likely to clash with the positively charged antibody paratope (Figures 6B and S5C). Such sites are especially difficult to identify by classical approaches such as alanine scanning, since the ability to escape neutralization is strongly dependent on which amino acid is introduced.

While the spatial clustering and biochemical evaluation of escape mutants suggest that they directly affect the interface between PGT151 and Env, it is possible that mutations indirectly affect neutralization by altering Env's conformation. To examine this possibility, we tested some of the most strongly selected PGT151 escape mutants with other bnAbs targeting the CD4 binding site and trimer apex. None of these mutations increased sensitivity to these other bnAbs targeting distal epitopes (Table S1). This fact strongly supports the idea that most PGT151 escape mutants that we have mapped directly disrupt the antibody-Env interface.

DISCUSSION

We have developed a massively parallel approach to interrogate the neutralization phenotype of all functionally tolerated single amino acid mutations to Env. We have used this approach to profile escape from PGT151, which targets a complex quaternary epitope. Our results recapitulate the escape mutations identified by previous low-throughput studies, reveal additional escape mutations not identified by these studies, and provide insight into the biochemical basis of escape.

Fine-resolution bnAb epitope mapping has previously been a cumbersome endeavor. Crystal structures of bnAb-Env complexes are often considered the gold standard, but can be difficult to obtain. In addition, the static structures do not reveal pathways of viral escape. Simply observing the evolution of HIV in the presence of a bnAb can identify specific escape mutations (Bar et al., 2016; Barouch et al., 2013; Diskin et al., 2013; Klein et al., 2012; Lynch et al., 2015a, 2015b; Shingai et al., 2013; Trkola et al., 2005), but the stochasticity of evolution means that each study only identifies one of potentially many pathways of escape. Functional residue-level mapping traditionally relies upon generating and testing Env mutants one by one, a resource-intensive approach that can only be applied to a fraction of Env mutations. For instance, such studies mostly restrict themselves to alanine mutations at surface sites, making them biased toward certain types of escape mutations. Therefore, despite the fact that PGT151 has been a subject of multiple studies using diverse techniques (Blattner et al., 2014; Falkowska et al., 2014; van Gils et al., 2016; Kong et al., 2016; Lee et al., 2016; Wibmer et al., 2017), our mutational antigenic profiling has yielded a far more comprehensive and unbiased map of viral escape than all this previous work.

This complete map offers a nuanced understanding of biochemical mechanisms of escape via evaluation of the physicochemical properties of the particular amino acid mutations that enable escape at each site. For instance, our data suggest that introduction of electrostatic clashes between the CDRH3 of PGT151 and the HR2 domain of gp41 is a previously unappreciated mechanism of escape. The specificity of escape at these sites contrasts with the many diverse amino acid mutations that were enriched at residue 647. This broad escape profile suggests that elimination of a key Env-PGT151 interaction underlies escape at site 647. The systematic quantification of the effect of each amino acid mutation at each site has the potential to augment structural studies by providing insight into the energetics of antibody-epitope interactions.

The ability to comprehensively map viral escape also has important application for bnAb-based immunotherapies and vaccines. Quantifying how epitope features contribute to neutralization could aid in engineering broader and more potent antibodies (Diskin et al., 2011). Such information could also inform the design of immunogens that elicit responses that thwart common pathways of viral escape. Completely defining viral determinants of escape will also aid in evaluating the efficacy and failure of bnAb immunotherapeutics in humans, just as determining drug resistance mutations has aided the development of antiviral therapy and prophylaxis (Lehman et al., 2015; Tural et al., 2002). Similar to algorithms that leverage large datasets of drug resistance mutations to predict antiviral resistance based on viral genotype (Vercauteren and Vandamme, 2006), comprehensive mutation-level escape profiles could inform similar sequence-based scoring metrics for bnAb resistance.

As with all epitope-mapping approaches, mutational antigenic profiling has limitations. We are evaluating the effects of single amino acid mutations to a single viral strain. Thus, this approach cannot reveal any potential synergistic effects of multiple mutations. Further, strain-specific differences in bnAb sensitivity have been described for PGT151 (Blattner et al., 2014; Falkowska

et al., 2014) and could explain why we did not observe escape at sites (533, 537, and 540) that have been shown to affect the sensitivity of JR-CSF to PGT151 (van Gils et al., 2016). Mutational antigenic profiling of escape from antibodies in multiple different Env isolates could determine the prevalence and mechanisms of such strain-specific differences. Lastly, we have assayed the enrichment of escape mutants at only a single strongly selective concentration of antibody. While our escape profiles accurately reflect values from TZM-bl neutralization assays, examining how mutation-level selection depends on antibody concentration is an interesting area for future work.

Few protein-protein interactions have been as heavily studied as those between bnAbs and Env. Indeed, these interactions provide the motivation for many current HIV treatment and prevention efforts. We have provided a complete map of the viral determinants of neutralization and escape at one of these bnAb-Env interfaces. The mutational antigenic profiling approach that we have used to obtain this map is high-throughput and quantitative. We anticipate that this approach can be extended to define all possible HIV escape mutations from other bnAbs and possibly polyclonal serum. The resulting maps could be valuable for informing the design of immunogens and the development and evaluation of bnAb immunotherapies.

STAR★METHODS

Detailed methods are provided in the online version of this paper and include the following:

- KEY RESOURCES TABLE
- CONTACT FOR REAGENT AND RESOURCE SHARING
- EXPERIMENTAL MODEL AND SUBJECT DETAILS
- METHODS DETAILS
  - Generation of Mutant DNA Libraries
  - Generation of Mutant Virus Libraries
  - PGT151 Selection of Mutant Virus Libraries
  - Deep Sequencing
  - Env Sequence Numbering
  - PGT151 Production
  - ddPCR Protocol
  - TZM-bl Neutralization Assays
  - Structural Analyses
- QUANTIFICATION AND STATISTICAL ANALYSIS
  - Computation of Differential Selection
  - TZM-bl Neutralization Curve Analyses
- DATA AND SOFTWARE AVAILABILITY
  - Data and Source Code

SUPPLEMENTAL INFORMATION

Supplemental Information includes five figures, one table, and six data files and can be found with this article online at http://dx.doi.org/10.1016/j.chom.2017.05.003.

AUTHOR CONTRIBUTIONS

Conceptualization, A.S.D., J.O., and J.D.B.; Methodology, A.S.D., H.K.H., and J.D.B.; Validation, A.S.D.; Investigation, A.S.D.; Software, A.S.D. and J.D.B.; Supervision, J.O. and J.D.B.; Writing – Original Draft, A.S.D.; Writing – Review & Editing, A.S.D., H.K.H., J.O., and J.D.B.; Funding Acquisition, J.O. and J.D.B.

ACKNOWLEDGMENTS

We thank James Hoxie for the SupT1.CCR5 cells, Michael Doud and Michael Emerman for helpful discussions, and Mark Pankau for assistance with ddPCR. We thank the Fred Hutch Genomics core for performing the Illumina sequencing. A.S.D. was supported by an NSF Graduate Research Fellowship (DGE-1256082). H.K.H. was supported by a Cell and Molecular Biology Training Grant (T32GM007270) and a Molecular Biophysics Training Grant (T32GM0008268). This work was supported by NIH grants R01GM102198 and R01AI127893 to J.D.B. and DA039543 and R01AI120961 to J.O. The research of J.D.B. was also supported in part by a Faculty Scholar Grant from the Howard Hughes Medical Institute and the Simons Foundation.

Received: March 21, 2017
Revised: April 27, 2017
Accepted: May 9, 2017
Published: June 1, 2017

REFERENCES

Baker, N.A., Sept, D., Joseph, S., Holst, M.J., and McCammon, J.A. (2001). Electrostatics of nanosystems: application to microtubules and the ribosome. Proc. Natl. Acad. Sci. USA *98*, 10037–10041.

Bar, K.J., Sneller, M.C., Harrison, L.J., Justement, J.S., Overton, E.T., Petrone, M.E., Salantes, D.B., Seamon, C.A., Scheinfeld, B., Kwan, R.W., et al. (2016). Effect of HIV antibody VRC01 on viral rebound after treatment interruption. N. Engl. J. Med. *375*, 2037–2050.

Barouch, D.H., Whitney, J.B., Moldt, B., Klein, F., Oliveira, T.Y., Liu, J., Stephenson, K.E., Chang, H.-W., Shekhar, K., Gupta, S., et al. (2013). Therapeutic efficacy of potent neutralizing HIV-1-specific monoclonal antibodies in SHIV-infected rhesus monkeys. Nature *503*, 224–228.

Benki, S., McClelland, R.S., Emery, S., Baeten, J.M., Richardson, B.A., Lavreys, L., Mandaliya, K., and Overbaugh, J. (2006). Quantification of genital human immunodeficiency virus type 1 (HIV-1) DNA in specimens from women with low plasma HIV-1 RNA levels typical of HIV-1 nontransmitters. J. Clin. Microbiol. *44*, 4357–4362.

Blattner, C., Lee, J.H., Sliepen, K., Derking, R., Falkowska, E., de la Peña, A.T., Cupo, A., Julien, J.-P., van Gils, M., Lee, P.S., et al. (2014). Structural delineation of a quaternary, cleavage-dependent epitope at the gp41-gp120 interface on intact HIV-1 Env trimers. Immunity *40*, 669–680.

Bloom, J.D. (2014). An experimentally determined evolutionary model dramatically improves phylogenetic fit. Mol. Biol. Evol. *31*, 1956–1978.

Bloom, J.D. (2015). Software for the analysis and visualization of deep mutational scanning data. BMC Bioinformatics *16*, 168.

Boyd, D.F., Peterson, D., Haggarty, B.S., Jordan, A.P.O., Hogan, M.J., Goo, L., Hoxie, J.A., and Overbaugh, J. (2015). Mutations in HIV-1 envelope that enhance entry with the macaque CD4 receptor alter antibody recognition by disrupting quaternary interactions within the trimer. J. Virol. *89*, 894–907.

Caskey, M., Klein, F., Lorenzi, J.C.C., Seaman, M.S., West, A.P., Jr., Buckley, N., Kremer, G., Nogueira, L., Braunschweig, M., Scheid, J.F., et al. (2015). Viraemia suppressed in HIV-1-infected humans by broadly neutralizing antibody 3BNC117. Nature *522*, 487–491.

Caskey, M., Schoofs, T., Gruell, H., Settler, A., Karagounis, T., Kreider, E.F., Murrell, B., Pfeifer, N., Nogueira, L., Oliveira, T.Y., et al. (2017). Antibody 10-1074 suppresses viremia in HIV-1-infected individuals. Nat. Med. *23*, 185–191.

Chakrabarti, L., Emerman, M., Tiollais, P., and Sonigo, P. (1989). The cytoplasmic domain of simian immunodeficiency virus transmembrane protein modulates infectivity. J. Virol. *63*, 4395–4403.

Clackson, T., and Wells, J.A. (1995). A hot spot of binding energy in a hormone-receptor interface. Science *267*, 383–386.

Cortez, V., Wang, B., Dingens, A., Chen, M.M., Ronen, K., Georgiev, I.S., McClelland, R.S., and Overbaugh, J. (2015). The broad neutralizing antibody responses after HIV-1 superinfection are not dominated by antibodies directed to epitopes common in single infection. PLoS Pathog. *11*, e1004973.

Crooks, G.E., Hon, G., Chandonia, J.-M., and Brenner, S.E. (2004). WebLogo: a sequence logo generator. Genome Res. *14*, 1188–1190.

Cunningham, B.C., and Wells, J.A. (1993). Comparison of a structural and a functional epitope. J. Mol. Biol. *234*, 554–563.

Diskin, R., Scheid, J.F., Marcovecchio, P.M., West, A.P., Jr., Klein, F., Gao, H., Gnanapragasam, P.N.P., Abadir, A., Seaman, M.S., Nussenzweig, M.C., and Bjorkman, P.J. (2011). Increasing the potency and breadth of an HIV antibody by using structure-based rational design. Science *334*, 1289–1293.

Diskin, R., Klein, F., Horwitz, J.A., Halper-Stromberg, A., Sather, D.N., Marcovecchio, P.M., Lee, T., West, A.P., Jr., Gao, H., Seaman, M.S., et al. (2013). Restricting HIV-1 pathways for escape using rationally designed anti-HIV-1 antibodies. J. Exp. Med. *210*, 1235–1249.

Doud, M.B., and Bloom, J.D. (2016). Accurate measurement of the effects of all amino-acid mutations on influenza hemagglutinin. Viruses *8*, 155.

Doud, M.B., Hensley, S.E., and Bloom, J.D. (2017). Complete mapping of viral escape from neutralizing antibodies. PLoS Pathog. *13*, e1006271.

Falkowska, E., Ramos, A., Feng, Y., Zhou, T., Moquin, S., Walker, L.M., Wu, X., Seaman, M.S., Wrin, T., Kwong, P.D., et al. (2012). PGV04, an HIV-1 gp120 CD4 binding site antibody, is broad and potent in neutralization but does not induce conformational changes characteristic of CD4. J. Virol. *86*, 4394–4403.

Falkowska, E., Le, K.M., Ramos, A., Doores, K.J., Lee, J.H., Blattner, C., Ramirez, A., Derking, R., van Gils, M.J., Liang, C.-H., et al. (2014). Broadly neutralizing HIV antibodies define a glycan-dependent epitope on the prefusion conformation of gp41 on cleaved envelope trimers. Immunity *40*, 657–668.

Goo, L., Milligan, C., Simonich, C.A., Nduati, R., and Overbaugh, J. (2012). Neutralizing antibody escape during HIV-1 mother-to-child transmission involves conformational masking of distal epitopes in envelope. J. Virol. *86*, 9566–9582.

Haddox, H.K., Dingens, A.S., and Bloom, J.D. (2016). Experimental estimation of the effects of all amino-acid mutations to HIV's envelope protein on viral replication in cell culture. PLoS Pathog. *12*, e1006114.

Hessell, A.J., Poignard, P., Hunter, M., Hangartner, L., Tehrani, D.M., Bleeker, W.K., Parren, P.W.H.I., Marx, P.A., and Burton, D.R. (2009). Effective, low-titer antibody protection against low-dose repeated mucosal SHIV challenge in macaques. Nat. Med. *15*, 951–954.

Horwitz, J.A., Halper-Stromberg, A., Mouquet, H., Gitlin, A.D., Tretiakova, A., Eisenreich, T.R., Malbec, M., Gravemann, S., Billerbeck, E., Dorner, M., et al. (2013). HIV-1 suppression and durable control by combining single broadly neutralizing antibodies and antiretroviral drugs in humanized mice. Proc. Natl. Acad. Sci. USA *110*, 16538–16543.

Jabara, C.B., Jones, C.D., Roach, J., Anderson, J.A., and Swanstrom, R. (2011). Accurate sampling and deep sequencing of the HIV-1 protease gene using a Primer ID. Proc. Natl. Acad. Sci. USA *108*, 20166–20171.

Jardine, J.G., Kulp, D.W., Havenar-Daughton, C., Sarkar, A., Briney, B., Sok, D., Sesterhenn, F., Ereño-Orbea, J., Kalyuzhniy, O., Deresa, I., et al. (2016). HIV-1 broadly neutralizing antibody precursor B cells revealed by germline-targeting immunogen. Science *351*, 1458–1463.

Klein, F., Halper-Stromberg, A., Horwitz, J.A., Gruell, H., Scheid, J.F., Bournazos, S., Mouquet, H., Spatz, L.A., Diskin, R., Abadir, A., et al. (2012). HIV therapy by a combination of broadly neutralizing antibodies in humanized mice. Nature *492*, 118–122.

Kong, R., Xu, K., Zhou, T., Acharya, P., Lemmin, T., Liu, K., Ozorowski, G., Soto, C., Taft, J.D., Bailer, R.T., et al. (2016). Fusion peptide of HIV-1 as a site of vulnerability to neutralizing antibody. Science *352*, 828–833.

Korber, B.T., Foley, B.T., Kuiken, C.L., Pillai, S.K., and Sodroski, J.G. (1998). Numbering positions in HIV relative to HXB2CG. Hum. Retroviruses AIDS *3*, 102–111.

Lee, J.H., Ozorowski, G., and Ward, A.B. (2016). Cryo-EM structure of a native, fully glycosylated, cleaved HIV-1 envelope trimer. Science *351*, 1043–1048.

Lehman, D.A., Baeten, J.M., McCoy, C.O., Weis, J.F., Peterson, D., Mbara, G., Donnell, D., Thomas, K.K., Hendrix, C.W., Marzinke, M.A., et al.; Partners PrEP Study Team (2015). Risk of drug resistance among persons acquiring HIV within a randomized clinical trial of single- or dual-agent preexposure prophylaxis. J. Infect. Dis. *211*, 1211–1218.

Li, Y., Luo, L., Thomas, D.Y., and Kang, C.Y. (1994). Control of expression, glycosylation, and secretion of HIV-1 gp120 by homologous and heterologous signal sequences. Virology *204*, 266–278.

Li, Y., O'Dell, S., Walker, L.M., Wu, X., Guenaga, J., Feng, Y., Schmidt, S.D., McKee, K., Louder, M.K., Ledgerwood, J.E., et al. (2011). Mechanism of neutralization by the broadly neutralizing HIV-1 monoclonal antibody VRC01. J. Virol. *85*, 8954–8967.

Lynch, R.M., Boritz, E., Coates, E.E., DeZure, A., Madden, P., Costner, P., Enama, M.E., Plummer, S., Holman, L., Hendel, C.S., et al.; VRC 601 Study Team (2015a). Virologic effects of broadly neutralizing antibody VRC01 administration during chronic HIV-1 infection. Sci. Transl. Med. *7*, 319ra206.

Lynch, R.M., Wong, P., Tran, L., O'Dell, S., Nason, M.C., Li, Y., Wu, X., and Mascola, J.R. (2015b). HIV-1 fitness cost associated with escape from the VRC01 class of CD4 binding site neutralizing antibodies. J. Virol. *89*, 4201–4213.

Margolis, D.M., Koup, R.A., and Ferrari, G. (2017). HIV antibodies for treatment of HIV infection. Immunol. Rev. *275*, 313–323.

Mascola, J.R., Lewis, M.G., Stiegler, G., Harris, D., VanCott, T.C., Hayes, D., Louder, M.K., Brown, C.R., Sapan, C.V., Frankel, S.S., et al. (1999). Protection of Macaques against pathogenic simian/human immunodeficiency virus 89.6PD by passive transfer of neutralizing antibodies. J. Virol. *73*, 4009–4018.

Mascola, J.R., Stiegler, G., VanCott, T.C., Katinger, H., Carpenter, C.B., Hanson, C.E., Beary, H., Hayes, D., Frankel, S.S., Birx, D.L., and Lewis, M.G. (2000). Protection of macaques against vaginal transmission of a pathogenic HIV-1/SIV chimeric virus by passive infusion of neutralizing antibodies. Nat. Med. *6*, 207–210.

McCoy, L.E., Falkowska, E., Doores, K.J., Le, K., Sok, D., van Gils, M.J., Euler, Z., Burger, J.A., Seaman, M.S., Sanders, R.W., et al. (2015). Incomplete neutralization and deviation from sigmoidal neutralization curves for HIV broadly neutralizing monoclonal antibodies. PLoS Pathog. *11*, e1005110.

Moldt, B., Rakasz, E.G., Schultz, N., Chan-Hui, P.-Y., Swiderek, K., Weisgrau, K.L., Piaskowski, S.M., Bergman, Z., Watkins, D.I., Poignard, P., and Burton, D.R. (2012). Highly potent HIV-specific antibody neutralization in vitro translates into effective protection against mucosal SHIV challenge in vivo. Proc. Natl. Acad. Sci. USA *109*, 18921–18925.

Parren, P.W.H.I., Marx, P.A., Hessell, A.J., Luckay, A., Harouse, J., Cheng-Mayer, C., Moore, J.P., and Burton, D.R. (2001). Antibody protects macaques against vaginal challenge with a pathogenic R5 simian/human immunodeficiency virus at serum levels giving complete neutralization in vitro. J. Virol. *75*, 8340–8347.

Pegu, A., Yang, Z.Y., Boyington, J.C., Wu, L., Ko, S.-Y., Schmidt, S.D., McKee, K., Kong, W.-P., Shi, W., Chen, X., et al. (2014). Neutralizing antibodies to HIV-1 envelope protect more effectively in vivo than those to the CD4 receptor. Sci. Transl. Med. *6*, 243ra88.

Pegu, A., Hessell, A.J., Mascola, J.R., and Haigwood, N.L. (2017). Use of broadly neutralizing antibodies for HIV-1 prevention. Immunol. Rev. *275*, 296–312.

Poignard, P., Sabbe, R., Picchio, G.R., Wang, M., Gulizia, R.J., Katinger, H., Parren, P.W.H.I., Mosier, D.E., and Burton, D.R. (1999). Neutralizing antibodies have limited effects on the control of established HIV-1 infection in vivo. Immunity *10*, 431–438.

Poss, M., and Overbaugh, J. (1999). Variants from the diverse virus population identified at seroconversion of a clade A human immunodeficiency virus type 1-infected woman have distinct biological properties. J. Virol. *73*, 5255–5264.

Provine, N.M., Puryear, W.B., Wu, X., Overbaugh, J., and Haigwood, N.L. (2009). The infectious molecular clone and pseudotyped virus models of human immunodeficiency virus type 1 exhibit significant differences in virion composition with only moderate differences in infectivity and inhibition sensitivity. J. Virol. *83*, 9002–9007.

Scheid, J.F., Horwitz, J.A., Bar-On, Y., Kreider, E.F., Lu, C.-L., Lorenzi, J.C.C., Feldmann, A., Braunschweig, M., Nogueira, L., Oliveira, T., et al. (2016). HIV-1

antibody 3BNC117 suppresses viral rebound in humans during treatment interruption. Nature *535*, 556–560.

Shingai, M., Nishimura, Y., Klein, F., Mouquet, H., Donau, O.K., Plishka, R., Buckler-White, A., Seaman, M., Piatak, M., Jr., Lifson, J.D., et al. (2013). Antibody-mediated immunotherapy of macaques chronically infected with SHIV suppresses viraemia. Nature *503*, 277–280.

Simonich, C.A., Williams, K.L., Verkerke, H.P., Williams, J.A., Nduati, R., Lee, K.K., and Overbaugh, J. (2016). HIV-1 neutralizing antibodies with limited hypermutation from an infant. Cell *166*, 77–87.

Steichen, J.M., Kulp, D.W., Tokatlian, T., Escolano, A., Dosenovic, P., Stanfield, R.L., McCoy, L.E., Ozorowski, G., Hu, X., Kalyuzhniy, O., et al. (2016). HIV vaccine design to target germline precursors of glycan-dependent broadly neutralizing antibodies. Immunity *45*, 483–496.

Strain, M.C., Lada, S.M., Luong, T., Rought, S.E., Gianella, S., Terry, V.H., Spina, C.A., Woelk, C.H., and Richman, D.D. (2013). Highly precise measurement of HIV DNA by droplet digital PCR. PLoS One *8*, e55943.

Todd, C.A., Greene, K.M., Yu, X., Ozaki, D.A., Gao, H., Huang, Y., Wang, M., Li, G., Brown, R., Wood, B., et al. (2012). Development and implementation of an international proficiency testing program for a neutralizing antibody assay for HIV-1 in TZM-bl cells. J. Immunol. Methods *375*, 57–67.

Trkola, A., Kuster, H., Rusert, P., Joos, B., Fischer, M., Leemann, C., Manrique, A., Huber, M., Rehr, M., Oxenius, A., et al. (2005). Delay of HIV-1 rebound after cessation of antiretroviral therapy through passive transfer of human neutralizing antibodies. Nat. Med. *11*, 615–622.

Tural, C., Ruiz, L., Holtzer, C., Schapiro, J., Viciana, P., González, J., Domingo, P., Boucher, C., Rey-Joly, C., and Clotet, B.; Havana Study Group (2002). Clinical utility of HIV-1 genotyping and expert advice: the Havana trial. AIDS *16*, 209–218.

van Gils, M.J., van den Kerkhof, T.L.G.M., Ozorowski, G., Cottrell, C.A., Sok, D., Pauthner, M., Pallesen, J., de Val, N., Yasmeen, A., de Taeye, S.W., et al. (2016). An HIV-1 antibody from an elite neutralizer implicates the fusion peptide as a site of vulnerability. Nat. Microbiol. *2*, 16199.

Vercauteren, J., and Vandamme, A.M. (2006). Algorithms for the interpretation of HIV-1 genotypic drug resistance information. Antiviral Res. *71*, 335–342.

Wibmer, C.K., Gorman, J., Ozorowski, G., Bhiman, J.N., Sheward, D.J., Elliott, D.H., Rouelle, J., Smira, A., Joyce, M.G., Ndabambi, N., et al. (2017). Structure and recognition of a novel HIV-1 gp120-gp41 interface antibody that caused MPER exposure through viral escape. PLoS Pathog. *13*, e1006074.

Wu, X., and Kong, X.-P. (2016). Antigenic landscape of the HIV-1 envelope and new immunological concepts defined by HIV-1 broadly neutralizing antibodies. Curr. Opin. Immunol. *42*, 56–64.

Wu, X., Parast, A.B., Richardson, B.A., Nduati, R., John-Stewart, G., Mbori-Ngacha, D., Rainwater, S.M.J., and Overbaugh, J. (2006). Neutralization escape variants of human immunodeficiency virus type 1 are transmitted from mother to infant. J. Virol. *80*, 835–844.

Wu, N.C., Du, Y., Le, S., Young, A.P., Zhang, T.-H., Wang, Y., Zhou, J., Yoshizawa, J.M., Dong, L., Li, X., et al. (2016). Coupling high-throughput genetics with phylogenetic information reveals an epistatic interaction on the influenza A virus M segment. BMC Genomics *17*, 46.

Yuste, E., Reeves, J.D., Doms, R.W., and Desrosiers, R.C. (2004). Modulation of Env content in virions of simian immunodeficiency virus: correlation with cell surface expression and virion infectivity. J. Virol. *78*, 6775–6785.

STAR★METHODS

KEY RESOURCES TABLE

REAGENT or RESOURCE	SOURCE	IDENTIFIER
Antibodies		
PGT151	Falkowska et al., 2014	GenBank: KJ700290.1 and KJ700282.1
Bacterial and Virus Strains		
BF520.W14.C2 *env*	Wu et al., 2006	GenBank: KX168094.1
Q23-17	Poss and Overbaugh, 1999	GenBank: AF004885.1
Q23.BsmBI.BF520.C2	This paper	N/A
ElectroMAX DH10B competent cells	Invitrogen	Cat. # 12033-015
Deposited Data		
Illumina deep sequencing data	NCBI Sequence Reads Archive	SRA: SRX2548567–SRX2548579
Experimental Models: Cell Lines		
SupT1.CCR5	James Hoxie	Boyd et al., 2015
TZM-bl	NIH AIDS Reagents; contributed by Dr. John C. Kappes, Dr. Xiaoyun Wu, and Tranzyme	Cat. # 8129
Oligonucleotides		
BF520.C2 *env* mutagenesis primers	This paper	Data S4
BF520.C2 barcoded subamplicon deep sequencing primers	This paper	Data S6
Recombinant DNA		
Q23.BsmBI.ΔEnv	This paper	Data S5
BF520.C2 mutant proviral libraries (n = 3)	This paper	N/A
Software and Algorithms		
dms_tools	Bloom, 2015	https://github.com/jbloomlab/dms_tools
Codon Tiling Primers	Bloom, 2014	https://github.com/jbloomlab/CodonTilingPrimers
PGT151 mutational antigenic profiling pipeline	This paper	https://github.com/adingens/BF520_MutationalAntigenicProfiling_PGT151

CONTACT FOR REAGENT AND RESOURCE SHARING

Further information and requests for resources and reagents should be directed to and will be fulfilled by the Lead Contact, Jesse Bloom (jbloom@fredhutch.org).

EXPERIMENTAL MODEL AND SUBJECT DETAILS

SupT1,CCR5 cells, a kind gift from Dr. James Hoxie, are SupT1 cells lentiviral transduced to express CCR5. SupT1 cells are a T cell lymphoblast originally isolated from 8 year old, Caucasian male with T cell lymphoblastic lymphoma. Cells were maintained as described in the Generation of mutant virus libraries at 37°C in the presence of 5% CO_2.

METHODS DETAILS

Generation of Mutant DNA Libraries

Codon mutant libraries were created in the context of BF520 *env* introduced into the full-length proviral clone Q23 (Poss and Overbaugh, 1999). Q23 is a subtype A transmitted/founder virus that is the basis for a well characterized system of generating chimeric full length proviral clones as well as pseudoviruses encoding heterologous *env* genes (Provine et al., 2009).

We first introduced codon mutations into *env* in three independent replicates using a slightly modified version of a previously described PCR mutagenesis technique (Bloom, 2014). However, we made one modification: to overcome potential biases in the frequency of introduced mutations, we used mutagenesis primers of equal melting temperature (of ≈60°C) rather than equal length.

These primers are provided as Data S4. We then cloned 4 × 10^5 – 1 × 10^6 unique variants of for each mutant *env* library into a high efficiency-cloning vector (Q23.BsmBI.ΔEnv; Data S5) that utilizes BsmBI restriction sites to clone *env* into the Q23 backbone. T4 DNA ligation products were transformed into ElectroMAX DH10B competent cells (Invitrogen; 12033-015). The next day, plated colonies were scraped, grown in LB plus ampicillin for 4 hr, and maxiprepped. The number of unique variants per library was determined by counting colonies on plates containing a dilution of the high efficiency transformation.

Generation of Mutant Virus Libraries

To generate mutant virus libraries, 36 μg total of each mutant DNA library was transfected using Fugene-6 into 18 wells of 6-well plates, that had been plated with 4 × 10^5 293T cells per well the previous day. Two days post transfection, supernatants were collected, filtered through a 0.2 uM filter, and DNase (Roche; 4716728001) treated to eliminate leftover transfection plasmid as previously described (Haddox et al., 2016). This transfection supernatant was then titered on TZM-bl cells by adding serial dilutions of the supernatant to 20,000 cells in the presence of 10 μg/mL DEAE-dextran in 600 μL total volume. After 48 hr, cells were fixed and stained for beta-galactosidase, and infected cell foci were counted.

To establish a genotype-phenotype link and select for functional variants, we passaged each mutant library for 4 days in SupT1.CCR5 cells at a low MOI (0.01 TZM-bl infectious units/cell). This initial passage in in SupT1.CCR5 cells was performed similarly to Haddox et al. (2016). We infected cells in with 3 × 10^6 (replicate 1) or 4 × 10^6 (replicates 2 and 3) infectious units of transfection supernatant in T-225 flasks, each with 100 mL total volume of R10 (RPMI [GE Healthcare Life Sciences; SH30255.01], supplemented with 10% FBS, 1% 200 mM L-glutamine, and 1% of a solution of 10,000 units/mL penicillin and 10,000 μg/mL streptomycin) in the presence of 10 μg/mL DEAE-dextran with cells starting at a concentration of 1 × 10^6 cells/mL. On day 1, we replaced the media with fresh R10 containing 10 μg/mL DEAE-dextran, and on day 2, we doubled the total volume, splitting each flask into two. On day 4, we pooled all the flasks, spun down cells, and filtered the media through a 0.2 μM filter. We then concentrated this virus ~33 fold via ultracentrifugation for 1 hr at 4°C at 23,000 RPM over a 20% sucrose cushion using an SW 28 rotor (Beckman Coulter; 342207) and resuspended in R10. In parallel for each replicate, we passaged 5 × 10^5 infectious units of wild-type virus under the same conditions as a control. These passaged viruses were titered on TZM-bl cells.

PGT151 Selection of Mutant Virus Libraries

We incubated each mutant virus library with PGT151 and infected SupT1.CCR5 cells again. Each library was also passaged without PGT151 treatment to serve as a replicate-specific control to calculate differential selection. For each condition, 10^6 TZM-bl infectious units of each library was incubated ± 1 μg/mL of PGT151 at 37°C for 1 hr, then infected into 10^6 (not PGT151 treated) or 2 × 10^5 (PGT151 treated) SupT1.CCR5 cells in the presence of 100 ug/mL DEAE-dextran. This concentration was chosen with the goal of inhibiting ~97.5% of the viral infectivity. Three hours post infection, cells were spun down and resuspended in fresh R10, containing no DEAE-dextran. At 12 hr post infection, cells were spun down, washed with PBS, and then subjected to a mini-prep to harvest non-integrated viral cDNA. We also infected non-neutralized wild-type virus in parallel for each library.

Deep Sequencing

To determine the frequency of each mutation in the antibody-selected and non-selected conditions, we utilized a barcoded subamplicon Illumina deep sequencing approach as previously described (Doud and Bloom, 2016; Haddox et al., 2016). This approach uses unique molecular identifiers to distinguish true mutation from sequencing errors. It reduced the error rate when sequencing wild-type proviral plasmid to 1.5 × 10^{-4} mutations per codon (Figure S2). Primers used during the sequencing library preparation are provided in Data S6. KOD Hot Start Master Mix (EMD Millipore, 71842) was used for each PCR reaction. PCR products were cleaned with Agencourt AMPure XP beads (Beckman Coulter, A63880) using a bead-to-sample ratio of 1.0 and quantified via Quant-iT PicoGreen dsDNA Assay Kit (Life Technologies, P7589) between each step in the library preparation process. Briefly, *env* was amplified from 20 μL of nonintegrated viral cDNA in a 50 μL reaction using the following thermocycler conditions:

1. 95°C, 2 min
2. 95°C, 20 s
3. 70°C, 1 s
4. 60°C, 10 s
5. 70°C, 2 min 4 s
6. Go to 2, repeat 27 times
7. Hold at 4°C

Next, 4 ng of *env* template was added to a 20 μL reaction supplemented with an additional 1 mM $MgCl_2$. This reaction was performed independently for each of the 6 subamplicons for each sample. This PCR reaction was:

1. 95°C, 2 min
2. 95°C, 20 s
3. 70°C, 1 s
4. 59°C, 10 s

5. 70°C, 10 s
6. Go to 2, repeat 10 times
7. 95°C for 1 min
8. Hold at 4°C

Next, ssDNA molecules were bottlenecked such that each molecule would be read, on average, ~2.7 times during Illumina sequencing. The 6 subamplicons for a single sample were then pooled, and a 20 μL PCR reaction, supplemented with an additional 1 mM $MgCl_2$, was performed to add the remainder of the Illumina sequencing adapters. This PCR reaction was:

1. 95°C, 2 min
2. 95°C, 20 s
3. 70°C, 1 s
4. 60°C, 10 s
5. 70°C, 10 s
6. Go to 2, repeat 23 times
7. Hold at 4°C

Finally, samples were pooled, purified by gel electrophoresis, and sequenced on an Illumina HiSeq or MiSeq using 2x250 bp paired-end reads. Figure S2C details the error-corrected sequencing depth per codon for each sample (roughly 10^5 unique error-corrected reads per codon for PGT151 selected samples).

Env Sequence Numbering

Unless otherwise stated, Env residues are numbered according to the HXB2 reference strain numbering system (Korber et al., 1998). The corresponding sequence numbering based on aligned BF520.W14M.C2 (GenBank: KX168094.1) and HXB2 env for the mutagenized portion of the gene is provided as Data S3.

PGT151 Production

PGT151 heavy (GenBank: KJ700282.1) and light (GenBank: KJ700290.1) chains were codon optimized, cloned into Igγ1 and Igκ expression vectors, and expressed in 293F cells using the FreeStyle MAX system (Invitrogen). IgG was purified using Protein G resin (Pierce; 20399) as described by Simonich et al. (2016).

ddPCR Protocol

To quantify the remaining infectivity of each mutant virus library after PGT151 selection and infection into SupT1.CCR5 cells, we used droplet-digital PCR. The number of viral genomes present in each harvested sample of viral cDNA was quantified using a pol PCR (Benki et al., 2006) adapted for digital droplet detection (Strain et al., 2013). The percent escape shown in Figure 2 was calculated using the number of genomes present in each selected library relative to its non-neutralized control.

TZM-bl Neutralization Assays

To validate our escape profiles, we generated pseudoviruses bearing individual point mutants of both enriched and non-enriched mutations. We then performed TZM-bl neutralization assays as previously described (Cortez et al., 2015) in the presence of 10 μg/mL DEAE-dextran. Briefly, serial dilutions of PGT151 were incubated with 500 TZM-bl infectious units of pseudovirus for one hour before the addition of 10,000 TZM-bl reporter cells in the presence of 10 μg/mL DEAE-dextran. Forty-eight hours post-infection, infectivity was read by beta-galactosidase activity using Gal-Screen (Thermo Fisher Scientific, T1028). Neutralization assays were performed in duplicate twice, and WT neutralization curves were run on each plate to reduce noise (Figure S4).

Structural Analyses

All structural analyses are based on the cryo-EM model of JR-FL EnvΔCT trimer bound by two PGT151 Fabs (Lee et al., 2016; PDB: 5FUU). For all figures, we focused on PGT151-Env interface 2 (Lee et al., 2016). Figures were generated using Pymol, and the Poisson-Boltzman electrostatic surface potential was calculated using the APBS plugin (Baker et al., 2001) with the protein dielectric constant of 20 for the trimer or PGT151 Fab (trimer bound conformation) in isolation.

QUANTIFICATION AND STATISTICAL ANALYSIS

Computation of Differential Selection

We calculated differential selection values as described in Doud et al. (2017). Briefly, the enrichment ($E_{r,x}$) of each amino acid x at site r relative to wild-type is calculated as shown in Equation 1, where $n_{r,x}^{mock}$ is the number of counts of x at site r in the mock treated sample. Similarly, $n_{r,x}^{selected}$ is the number of counts of x at site r in the PGT151 selected sample. $wt(r)$ is the wild-type character at r.

$$E_{r,\,x} = \frac{\left(n_{r,x}^{selected} + f_{r,\,selected} \times P\right) \Big/ \left(n_{r,wt(r)}^{selected} + f_{r,\,selected} \times P\right)}{\left(n_{r,x}^{mock} + f_{r,\,mock} \times P\right) \Big/ \left(n_{r,wt(r)}^{mock} + f_{r,\,mock} \times P\right)}. \quad \text{(Equation 1)}$$

To account for statistical noise associated with low counts, a pseudocount of $P = 20$ was added to each count. The $f_{r,selected}$ (Equation 2) and $f_{r,mock}$ (Equation 3) variables scale the pseudocount to account for different sequencing depth of the *mock* and *selected* libraries at site *r*.

$$f_{r,selected} = \max\left[1,\ \left(\sum_x n_{r,x}^{selected}\right) \Big/ \left(\sum_x n_{r,x}^{mock}\right)\right] \text{ and} \quad \text{(Equation 2)}$$

$$f_{r,mock} = \max\left[1,\ \left(\sum_x n_{r,x}^{mock}\right) \Big/ \left(\sum_x n_{r,x}^{selected}\right)\right]. \quad \text{(Equation 3)}$$

To account for errors in viral replication and sequencing, counts in Equation 1 were adjusted by the rates of mutation to *x* at site *r* in mock selected wild-type virus libraries passaged in parallel for each replicate. We define $n_{r,x}^{err}$ as the number of counts of *x* at site *r* in the matched wild-type virus control and $\varepsilon_{r,x}$ as shown in Equation 4, such that $\varepsilon_{r,x}$ is the rate of errors to *x* at site *r* when $x \neq wt(r)$, and $\varepsilon_{r,x}$ is one minus the rate of errors away from wild-type at site *r* when $x = wt(r)$ as defined in Equation 4.

$$\varepsilon_{r,x} = \frac{n_{r,x}^{err}}{\sum_y n_{r,y}^{err}}. \quad \text{(Equation 4)}$$

The observed counts in Equation 1 are then adjusted to the error-corrected counts $\widehat{n}_{r,x}$ as described in Equation 5.

$$\widehat{n}_{r,x} = \begin{cases} \max\left[\left(\sum_y n_{r,y}\right)\left(\frac{n_{r,x}}{\sum_y n_{r,y}} - \varepsilon_{r,x}\right), 0\right] & \text{if } x \neq wt(r) \\ n_{r,x} \big/ \varepsilon_{r,x} & \text{if } x = wt(r). \end{cases} \quad \text{(Equation 5)}$$

Lastly, differential selection values $s_{r,x}$ for *x* at *r* in the *selected* versus *mock* condition is quantified as $s_{r,x} = \log_2 E_{r,x}$, and visualized on logoplots rendered by dms_tools via weblogo (Crooks et al., 2004). Throughout this manuscript, we focused only on positively enriched mutations.

TZM-bl Neutralization Curve Analyses

TZM-bl neutralization curves were fit using 3-parameter nonlinear regression of the % neutralization values across the dilution series, with the bottom plateau constrained to 0 (Figure S4). To calculate the IC_{50} relative to wild-type, curves were solved for y = 50% neutralization. The fitted top plateau, averaged across replicates, is the maximum percent neutralization. Fold change in IC_{50} relative to WT was calculated within a single experiment and then averaged across replicates.

DATA AND SOFTWARE AVAILABILITY

Data and Source Code

Data were analyzed using dms_tools (Bloom, 2015) version 1.1.20 as described in the iPython notebook computational pipeline provided in Data S1 and available at https://github.com/adingens/BF520_MutationalAntigenicProfiling_PGT151. The software used to align sequence reads and compute differential selection is available at https://github.com/jbloomlab/dms_tools (Bloom, 2015). The deep sequencing data are available on the Sequence Read Archive under accession numbers SRA: SRX2548567–SRX2548579, and the mutation differential selection values are provided as Data S2.

The script used to generate the codon tiling mutagenesis primers is available at https://github.com/jbloomlab/CodonTilingPrimers.